Density Functional Calculations on Alanine-Derived Radicals: Influence of Molecular Environment on EPR Hyperfine Coupling Constants

E. Pauwels,* V. Van Speybroeck, P. Lahorte,‡ and M. Waroquier

Laboratory of Theoretical Physics, Universiteit Gent, Proeftuinstraat 86, B-9000 Gent, Belgium

Received: March 22, 2001; In Final Form: June 14, 2001

The amino acid L-α-alanine and its associated radiation-induced radicals display particular characteristics in solid-state that make it very appropriate for use in Electron Paramagnetic Resonance (EPR) dosimetry. In contrast to the number of experimental studies, relatively few theoretical studies have been published concerning the EPR parameters of these radicals. However, these studies inadequately account for the molecular environment of the alanine radicals in the crystalline lattice. Here, we present Density Functional Theory (DFT) calculations on one of the stable radiation-induced radicals of L-α-alanine both in molecular cluster models and in periodic models. An extensive investigation is presented on the various geometrical ingredients which have a substantial impact on the hyperfine coupling constants as the planarity of the radical backbone and the internal rotations of the final methyl and amino group vary. It is found that the accurate modeling of the hydrogen bonds with neighboring molecules is of utmost importance for an adequate reproduction of the experimental data.

1. Introduction

The amino acid L-α-alanine is one of the most intensively studied amino acids, mainly because of the properties it displays in the solid-state form. More specifically, upon irradiation of solid alanine, a variety of stable radicals is produced within the lattice. Because of good dose-yield factors, a linear signal response over a wide range of radiation doses, excellent fading characteristics and a small dependency of temperature, humidity, and other environmental factors, these radicals are ideally suited for Electron Paramagnetic Resonance (EPR) dosimetry.[1] As a result, numerous EPR and Electron Nuclear DOuble Resonance (ENDOR) studies on L-α-alanine have produced a large amount of experimental data concerning the electronic g-factor and the hyperfine coupling constants (hfcc's) of magnetic nuclei in alanine-derived radicals.[2]

It has been commonly assumed that the solid-state radical population of L-α-alanine at room temperature consisted of only one radical type, the so-called Stable Alanine Radical (SAR) or R1 as shown in Figure 1, and that all variations in the EPR spectrum could be ascribed to various properties of this radical.[3] This radical is formed by deamination from a protonated alanine radical anion, and was first detected in a single crystal by van Roggen et al.[4] and later refined by Miyagawa et al.[5] Speculations had been made on the possible coexistence of several stable radical species.[6] Only recently however, Sagstuen et al.[7] presented compelling experimental evidence in a combined EPR, ENDOR and ENDOR−Induced EPR (EIE) study of irradiated solid-state alanine for the existence of two more radiation-induced radicals, R2 and R3 (Figure 1). The figure also includes the primary radical anion which can only be observed at low temperature (77 K). Radical R2 is a hydrogen-abstraction product, and contributes substantially (40%) to the solid-state radical population, while R1 is the most found species (60%).[7] Radical R3 is a minority species, which is produced by hydrogen-abstraction followed by proton-transfer. In this study, we will focus on model systems of the radical R2 in the presence of its molecular environment in the crystal lattice, as it is the simplest adduct of alanine. The abstracted hydrogen is expected to disturb the crystal lattice in a minor way.

Alanine, as all other amino acids, adopts the zwitterionic form in the crystalline state and in solution. Upon irradiation, zwitterionic radicals are formed. Numerous theoretical studies have been performed on amino acids and their derived radicals in the zwitterionic form.[8] High-level ab initio calculations on the simplest amino acid, glycine, have shown that the zwitterionic form is not the energetically most favored structure in vacuo. Instead, the molecule undergoes intramolecular proton transfer from the amino group to one of the oxygen atoms to adopt the nonionic form.[9] Correspondingly, Barone and Adamo showed that the zwitterionic form for an isolated glycine radical does not correspond to a stationary point.[10] Consequently, to study amino acids like alanine or one of its derived radicals in solid state or solution, it is essential to account for intermolecular environmental effects.

Recently, ab initio Density Functional Theory (DFT) calculations have been carried out to calculate the hfcc's of selected nuclei in radicals of organic crystals in general[11] and alanine-derived radicals in specific. Lahorte et al.[12] performed calculations on alanine radicals in vacuo, where the radical structures were proposed from the experimentally available atomic positions of undamaged alanine[13] and constrained geometry optimizations had to be performed on this structure in order to prevent the intramolecular hydrogen transfer. Ban et al.[14] kept the radicals in their zwitterionic forms during geometry optimization by using a continuum model.[15] In this Onsager model, the radical under study is placed in a cavity surrounded by a continuum with a uniform dielectric constant.

* To whom all correspondence should be addressed. Fax: 32 (0)9 264 65 42. E-mail: ewald.pauwels@rug.ac.be.

‡ Laboratory of Subatomic and Radiation Physics, Radiation Physics Group.

10.1021/jp0110657 CCC: $20.00
Published on Web 08/18/2001

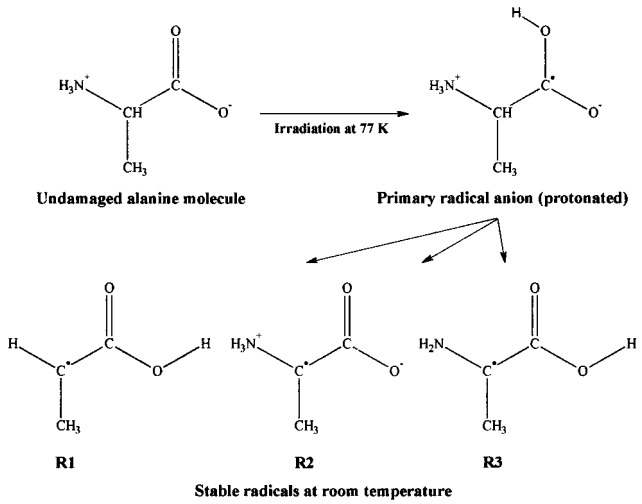

Figure 1. L-α-Alanine and derived radicals.

Although the environmental modeling in both approaches of Ban[14] and Lahorte[12] is inadequately described or even completely omitted, both studies succeed in reproducing in a satisfactory way the experimental isotropic hfcc's values, but only after adopting some crucial but acceptable assumptions. The agreement is only achieved after rotating the amino group about a specific angle. This assumption accounts for the missing environmental forces in the models, such as hydrogen bridges, but they remain speculative and deserve a more elaborate study by taking into account an adequate modeling of the crystalline environment. It might be expected that the neighboring molecules will affect the geometry of the radicals in the solid state and hence the hyperfine coupling constants.

In this paper, the environment is modeled by placing discrete molecules around the target radical. This should, in principle, allow for a straightforward determination of the correct geometry and conformation of the radical in the crystal lattice, by explicitly accounting for hydrogen bonds and other environmental forces. To this purpose we will adopt two approaches.

(i) The first approach is the cluster model, undoubtedly one of the most appropriate and successful methods for studying the condensed phase. It was first introduced by Saebo et al.[16] in its simplest form, where a central molecule was surrounded by atomic point charges, in positions as determined by an X-ray study. This simple point charge model has been extensively used, with relative success, to simulate the effects of the crystalline environment on a central molecule.[17] However, this model can only account for the long-range electrostatic interactions, but neglects the short-range overlap between the central molecule and its nearest neighbors.[18] A complete quantum mechanical treatment of both the central molecule and the environment is desired to model the intermolecular interactions correctly. This 'supermolecule' model has been used in this study to obtain an accurate geometry of the radical R2 embedded in a crystalline environment.

(ii) In the second approach explicit periodic calculations are performed on the crystal lattice. A simulated annealing technique, proposed by Car and Parrinello,[19] is used to minimize simultaneously the electronic and nuclear degrees of freedom. In this case the molecular environment is modeled in a full ab initio way, without introducing artificial boundaries.

The paper is organized as follows: in the next section we report on the computational details of both the cluster model and the periodic calculations. Section 3 gives an overview of the results. In a first part, we examine the influence of the environment on the geometry of the studied radical. The two ingredients which are primordial in the description of the global system—central radical and environment—are the model space and the level of theory. Their role on the various geometrical parameters will be reported and discussed. In the next part of this section the isotropic and anisotropic hfcc's of the magnetic nuclei in the radical R2 are reported for all optimized geometries. A detailed comparison of the theoretical predicted hfcc's with experimental values will be performed. Finally, some general conclusions are made.

2. Computational Details

In this study, we make use of two models which are essentially different in nature: the molecular-cluster model and the plane-wave model based upon periodic boundary conditions. This section deals with the computational details of both models, and elaborates on the method used for calculating the isotropic and anisotropic parts of the hyperfine coupling tensor.

2.1. Cluster Model. The radical of interest, R2, was surrounded by alanine molecules according to the space group symmetry $P_{2_1 2_1 2_1}$ of the L-α-alanine crystal.[13] The unit cell contains four alanine molecules and has unit cell constants of $a = 6.025$ Å, $b = 12.324$ Å, and $c = 5.783$ Å. Both the number of neighbors taken into account and the level of theory at which they are described were varied. Table 1 gives a schematic overview of all applied methods, and their short abbreviations for later reference. The methods used in earlier theoretical calculations[12,14] are also added for comparison.

In a first set of calculations, a cluster model of 15 L-α-alanine molecules was built in accordance with the appropriate space group symmetry. This model space was obtained by considering all surrounding molecules with at least one atom in one of the spheres with radius 3.7 Å, encircling every atom of the central radical. Finally, one hydrogen atom was abstracted from the central alanine molecule to obtain a starting geometry for radical R2. The methods, labeled PM3/PM3/14, B3LYP/PM3/14, and B3LYP/AM1/14 in Table 1, are based on this nearest- neighboring cluster model.

In a second set of calculations, the number of neighbors was reduced to six. Only those molecules are retained that are engaged in hydrogen bonds with atoms of the central radical. The structure of this hydrogen-bond cluster model is shown in Figure 2. Six hydrogen bonds are observed between the

TABLE 1: Overview of Applied Methods and Their Shortcut for Later Reference

	central radical	surrounding alanine cluster	notation
G98	PM3	14 molecules, PM3	PM3/PM3/14
G98	PM3	6 molecules, PM3	PM3/PM3/6
G98	B3LYP/6-31G**	14 molecules, PM3	B3LYP/PM3/14
G98	B3LYP/6-31G**	6 molecules, PM3	B3LYP/PM3/6
G98	B3LYP/6-31G**	14 molecules, AM1	B3LYP/AM1/14
G98	B3LYP/6-31G**	6 molecules, AM1	B3LYP/AM1/6
ADF	BLYP/I	6 molecules, BLYP/I	BLYP/I/6
ADF	BLYP/II	6 molecules, BLYP/II	BLYP/II/6
ADF	BLYP/III	6 molecules, BLYP/III	BLYP/III/6
AIMD	BP86/PW	15 molecules, BP86/PW	BP86/PW
G94	B3LYP/6-31G*	0 molecules	B3LYP/0/0[a]
G94	B3LYP/6-31+G**	Onsager water-model, 0 molecules	B3LYP/Onsager/0[a]

[a] B3LYP/0/0 and B3LYP/Onsager/0 refer to earlier theoretical calculations by Lahorte et al.[12] and Ban et al.[14]

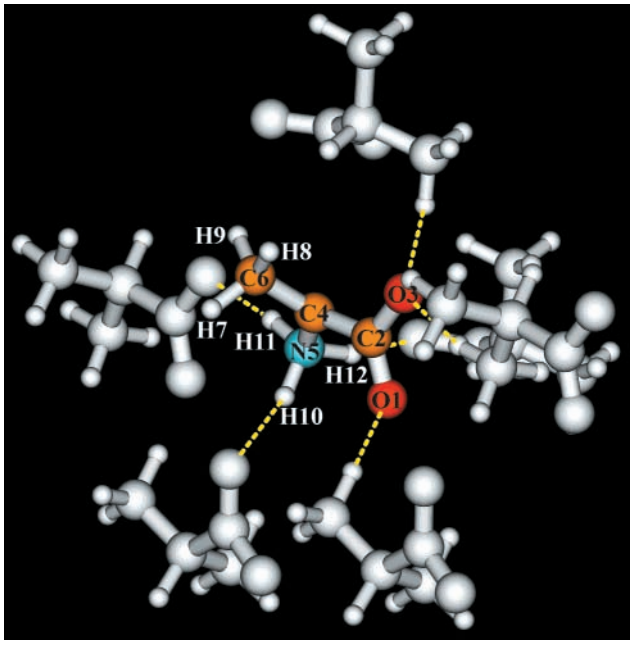

Figure 2. Optimized geometry of radical R2 and its neighboring L-α-alanine molecules, calculated at the B3LYP/PM3/6 level of theory.

hydrogen and oxygen atoms of the central radical and those of the neighboring alanine molecules. The methods PM3/PM3/6, B3LYP/PM3/6, B3LYP/AM1/6, BLYP/I/6, BLYP/II/6, and BLYP/III/6 refer to this second cluster model.

For both large (14 neighbors) as medium−large (6 neighbors) clusters, full geometry optimizations were performed on the central radical, while keeping the coordinates of the surrounding alanine molecules fixed in space at the experimental geometry.[13] The level of theory describing the central radical and its surrounding molecules is varied to determine its influence on the optimized geometry of the central radical.

Ab initio modeling of chemical systems with a large number of atoms on a high accurate level often poses numerical problems due to the limits of computational resources. One way to circumvent this problem is to use a simplified Hamiltonian, as in semiempirical and molecular mechanics methods.[20] In the models labeled PM3/PM3/6 and PM3/PM3/14, the full system was described by a semiempirical PM3 Hamiltonian[21] as implemented in the Gaussian 98 package.[22]

Although these methods are very attractive from a computational point of view, their empirical input limits their general applicability.[20] Full ab initio treatment of the cluster is more widely applicable, but is unfortunately very time-consuming. A possible solution to this problem is the use of hybrid methods: the cluster model under study is subdivided into several parts or layers, each described at a different level of theory. The interesting parts of the system—the "inner" layers—are treated at a high level of theory; the rest of the system—the "outer" layers—are described by a computationally less demanding method. In our study we employed a two-layered ONIOM approach[23]—also implemented in the Gaussian 98 software package—where the inner layer consists of the central radical R2. This part of the system was described within the Density Functional Theory (DFT)[24] framework by using Becke's three-parameter hybrid B3LYP functional.[25] Several studies[26] have indicated that this functional gives a reliable description of the geometry of a radical. The molecular orbitals were expanded in a double-ζ 6-31G split valence basis augmented with single d- and p-polarization functions.[27] The outer layer, consisting of 6 or 14 alanine molecules, was treated at the semiempirical level, either using a PM3 Hamiltonian[21] or an AM1 Hamiltonian.[28] These "layered" methods are referred to as B3LYP/PM3/6, B3LYP/PM3/14, B3LYP/AM1/6, and B3LYP/AM1/14.

In addition, we present in this work full ab initio calculations. However, due to the computational demand of such an exact treatment, only the cluster with six surrounding molecules is considered. For this type of calculations we used the Amsterdam Density Functional program (ADF1999) developed by Baerends et al.,[29] as similar calculations performed with the Gaussian 98 software package posed some serious convergence problems in the SCF procedure. All the atoms of the system were described within a DFT framework with the use of Becke's nonlocal exchange potential,[30] combined with a correlation potential as proposed by Lee, Yang, and Parr.[31] Basis sets of increasing size (and quality) were introduced to describe the molecular orbitals in a series of calculations, labeled by BLYP/I/6, BLYP/II/6, and BLYP/III/6. The basis sets I, II, and III in the ADF nomenclature employ Slater-type orbitals as basis functions. The sets I, II, and III correspond roughly to a single-ζ basis set, a double-ζ basis set and a double-ζ basis set extended with polarization functions, respectively. To accelerate SCF convergence, we used the electron-smearing option:[32] electrons were smeared out in an interval of 0.02 au over orbitals that lie around the Fermi level.

2.2. Periodic Calculations. In the second approach—which shall be referred to as BP86/PW—the crystal phase was modeled by performing periodic calculations. The crystal lattice of L-α-alanine is experimentally well characterized.[13] To simulate a radical R2 in the crystal lattice, we doubled the unit cell in the a and c direction to ensure that the radical defects are well separated from each other. The resulting orthorhombic unit cell contains 15 alanine molecules and a central R2 radical, as is

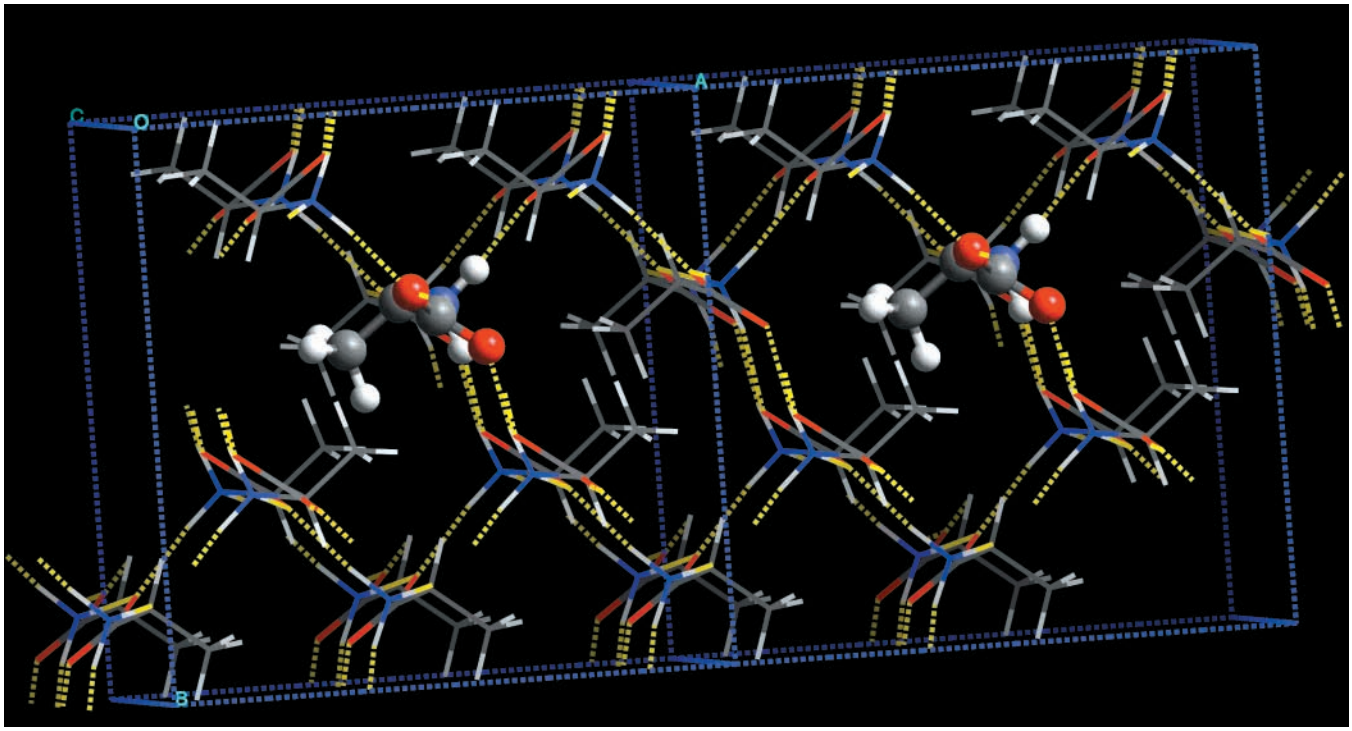

Figure 3. Optimized geometry of radical R2 and its neighboring L-α-alanine molecules in the periodic calculation, using plane waves and the BP86 density functional.

shown in Figure 3. The software package used for these calculations is the Ab Initio Quantum Molecular Dynamics (AIMD) Package[33] based on the Car−Parrinello code.[34] This algorithm was first proposed in a broader context of molecular dynamics simulations, with interatomic forces calculated "on the fly" from the instantaneous electronic potential. In this paper, the simulated annealing technique was used for the simultaneous optimization of the electronic and nuclear degrees of freedom toward a global energy minimum. This optimization scheme is based on a conjugate gradient minimization of the energy functional.[35] In our calculations only the structure of the radical was optimized, while the coordinates of all other atoms of surrounding alanine molecules were kept fixed at the experimental geometry by use of the SHAKE algorithm.[36]

The quantum mechanical description of the electronic structure is based on the DFT formalism. The exchange-correlation energy functional is treated within the local density approximation (LDA)[37] for which we employed the Perdew−Zunger parametrization for the homogeneous electron gas.[38] In addition, gradient corrections were included according to the schemes proposed by Perdew[39] and Becke,[40] known as BP86. Only valence electrons are treated explicitly and their corresponding single-particle orbitals are expanded in plane waves. Very soft pseudopotentials of the Vanderbilt type[41] are used to account for the core. An energy cutoff of 25 Ry (1 Ry = 1314 kJ/mol) is taken for the plane-wave expansion. Several other studies[42] have shown that this value is sufficient to describe the structure accurately.

2.3. EPR Hyperfine Coupling Constants. EPR hyperfine coupling constants represent the interaction between a nuclear spin and the electronic magnetic moments. This interaction is included in the spin Hamiltonian, which carries all interactions taking place in the molecular system as resulting from the presence of a magnetic field. For an organic paramagnetic system characterized by an electronic spin $S = 1/2$ and nuclear angular moment $I = 1/2$, the general expression for this Hamiltonian can be simplified to

$$H = \boldsymbol{\beta}_e \mathbf{H}\cdot\mathbf{g}\cdot\mathbf{S} - g_n\beta_n\mathbf{I}\cdot\mathbf{H} + \mathbf{S}\cdot\mathbf{A}\cdot\mathbf{I} \qquad (1)$$

The first two terms reflect the electronic and nuclear Zeeman contributions arising from the interaction of the external magnetic field **H** and the magnetic moments of the electrons and nuclei, specified by **S** and **I**, respectively. β_e, β_n and g_n are the Bohr magneton, the nuclear magneton, and the nuclear magnetogyric ratio; **g** is the so-called g-tensor. The hyperfine interaction matrix **A** in the last term of the spin Hamiltonian can be divided into an isotropic part and an anisotropic part. The isotropic part of the hyperfine matrix arises from coupling between the magnetic moments of the electrons *i* and the nucleus *n* through a contact interaction. It depends solely on the unpaired spin density $\sum_{\mu,\nu} P_{\mu,\nu}^{\alpha-\beta}$ at the position of the nucleus. This is shown in the following equation, assuming the g-tensor is isotropic:

$$A_{\mathrm{iso}}^{n} = \frac{8\pi}{3} g\beta_e g_n \beta_n \sum_{\mu,\nu} P_{\mu,\nu}^{\alpha-\beta} \langle \varphi_\mu(r_{ni}) | \delta(r_{ni}) | \varphi_\nu(r_{ni}) \rangle \qquad (2)$$

The anisotropic part of the hyperfine matrix is due to the interaction of magnetic dipoles, and is described by the following equation:

$$A_{uv}^{n} = g\beta_e g_n \beta_n \sum_{\mu,\nu} P_{\mu,\nu}^{\alpha-\beta} \langle \varphi_\mu(r_{ni}) | r_{ni}^{-5} (r_{ni}^2 \delta_{uv} - 3 r_{ni,u} r_{ni,v}) | \varphi_\nu(r_{ni}) \rangle \qquad (3)$$

for the uvth component.

Computation of both terms is already included in most ab initio codes. There are numerous examples available in the literature that have successfully calculated EPR hyperfine coupling constants in such way.[43] In this study, the hfcc's were calculated for all optimized geometries using the Gaussian 98

TABLE 2: Summary of Selected Geometrical Parameters for the Various Optimized Geometries

	B3LYP/ 0/0	B3LYP/ Onsager/0	PM3/PM3/ 14	PM3/PM3/ 6	B3LYP/ PM3/14	B3LYP/ PM3/6	B3LYP/ AM1/14	B3LYP/ AM1/6	BLYP/ I/6	BLYP/ II/6	BLYP/ III/6	BP86/ PW
Bond Lengths[a]												
O1−C2	1.271	1.277	1.254	1.251	1.261	1.264	1.272	1.277	1.335	1.317	1.278	1.285
C2−O3	1.242	1.295	1.264	1.272	1.282	1.292	1.270	1.277	1.399	1.339	1.302	1.307
C2−C4	1.511	1.507	1.507	1.500	1.466	1.455	1.468	1.464	1.540	1.450	1.465	1.467
C4−N5	1.492	1.478	1.460	1.458	1.503	1.503	1.465	1.466	1.563	1.489	1.472	1.464
C4−C6	1.479	1.478	1.463	1.461	1.487	1.484	1.478	1.475	1.547	1.492	1.484	1.483
H7−C6	1.102	1.100	1.105	1.099	1.107	1.103	1.104	1.101	1.118	1.110	1.107	1.114
H8−C6	1.093	1.090	1.103	1.097	1.094	1.090	1.092	1.087	1.105	1.096	1.093	1.103
H9−C6	1.102	1.100	1.102	1.133	1.102	1.107	1.104	1.112	1.110	1.104	1.102	1.106
H10−N5	1.023	1.030	1.024	1.005	1.058	1.053	1.044	1.040	1.100	1.047	1.043	1.064
H11−N5	1.025	1.030	1.025	1.015	1.055	1.051	1.038	1.034	1.125	1.057	1.054	1.109
H12−N5	1.037	1.052	1.024	1.025	1.052	1.057	1.039	1.043	1.222	1.076	1.078	1.054
Bond Angles												
O1−C2−O3	132.98	128.10	120.62	118.04	126.70	124.90	127.08	125.02	117.71	121.81	123.85	124.16
O1−C2−C4	111.27	113.50	116.96	120.62	116.40	118.18	116.21	117.35	127.63	119.11	117.94	116.19
C2−C4−N5	108.37	111.40	116.22	115.25	112.66	114.22	112.18	113.29	116.39	115.69	115.51	114.78
C2−C4−C6	131.77	130.20	122.05	124.07	124.52	126.72	128.41	128.94	114.74	125.74	125.12	119.59
Dihedral Angles												
O1−C2−C4−C6	180.00	180.00	122.73	120.47	115.27	125.69	153.77	163.76	99.51	137.81	134.40	114.67
O3−C2−C4−C6	0.00	0.00	−59.88	−63.95	−66.18	−55.55	−28.16	−17.32	−83.88	−42.96	−46.03	−61.55
H8−C6−C4−C2	0.00	0.00	26.21	351.25	34.62	23.13	9.22	355.62	42.47	8.97	14.10	42.56
H10−N5−C4−C2	82.40	79.00	82.39	80.40	71.04	73.45	10.79	10.77	60.36	77.76	75.20	71.77
Improper Torsion Angles												
O1−O3−C4−C2	0.00	0.00	1.52	2.47	0.83	0.70	1.11	0.62	1.69	0.44	0.24	2.21
C2−N5−C6−C4	0.00	0.00	6.60	1.57	17.22	11.62	1.22	−4.79	25.99	7.70	9.88	20.14
Hydrogen Bond Distances[b]												
O1−H*	?	?	1.84	1.83	1.87	1.86	2.13	2.13	1.61	2.10	2.10	2.01
O3−H*	?	?	1.78	1.73	1.78	1.80	1.91	1.94	1.79	1.74	1.76	1.78
O3−H*	?	?	1.81	1.74	1.79	1.76	1.95	1.97	1.47	1.74	1.74	1.49
H10−O*	?	?	1.84	2.51	1.81	1.87	2.70	2.93	2.04	1.94	1.99	1.83
H11−O*	?	?	1.76	1.76	1.76	1.79	2.47	2.52	1.75	1.75	1.77	1.52
H12−O*	?	?	1.83	1.75	1.83	1.78	2.38	2.28	1.37	1.71	1.68	1.85

[a] Units of bond lengths are angstroms. [b] The H* and O* symbols refer to one of the nearest hydrogen or oxygen atoms of the surrounding molecules.

software package[22] within the DFT framework. The B3LYP[25] functional was used and all atoms were assigned a triple-ζ 6-311G basis augmented with single first d- and p-polarization functions.[44] Recent studies indicate that a DFT procedure with a BLYP or B3LYP functional is to be preferred when calculating isotropic hfcc's of organic radicals.[45]

3. Results and Discussion

3.1. Geometry. As mentioned in section 2, geometry optimizations were performed at various levels of theory on the radical R2. In Table 2 a summary of selected geometrical parameters is given for the various optimized geometries. We also report on the geometries predicted by Lahorte et al.[12] and Ban et al.[14] These parameters include bond lengths, selected bond and dihedral angles, and hydrogen-bond distances. The position of the amino and methyl group relative to the rest of the central radical is given by the dihedral angles $H_{10}-N_5-C_4-C_2$ and $H_8-C_6-C_4-C_2$ respectively. The other hydrogen atoms lie in planes that form approximately 120° or 240° with respect to the (H_{10},N_4,C_4) and (H_8,C_6,C_4) planes for the amino- and methyl group, respectively. No bond angles involving hydrogen atoms are mentioned as they lie all around 110°. We also report on two "improper" torsion angles, namely $O_1-O_3-C_4-C_2$ and $C_2-N_5-C_6-C_4$. The first angle is a measure of deviation from planarity of the C2 carbon center. All optimized geometries point toward an almost planar conformation (see Table 2). The second improper torsion angle $C_2-N_5-C_6-C_4$ indicates the deviation from planarity of the radical backbone which is formed by the atoms N_5, C_4, C_6, and C_2. It accounts for a measure of sp^3 character of the radical center C_4. It turns out that all optimized geometries deviate from planarity but that the deviation largely depends on the employed level of theory. The maximum deviation amounts to 26° in the BLYP/I/6 optimized geometry, while only 1.2−1.6° in B3LYP/AM1/14 and PM3/PM3/6. On average, the deviation from planarity remains almost 7° and this is remarkable as it was previously always assumed in both experimental and theoretical studies, that upon hydrogen abstraction from C_4, the carbon atom transforms from an sp^3 to a perfectly planar sp^2 center. Our calculations do not support this picture. The interactions with the neighboring molecules force the central radical into a nonplanar conformation. This nonplanarity of the radical backbone can be clearly seen in Figure 2, displaying the optimized geometry at the B3LYP/PM3/6 level, and in Figure 3 as well, showing the results of the periodic calculation.

We notice a strong correlation between the nonplanarity of the radical backbone and the rotation of the CO_2 group relative to the reference (C_2,N_5,C_6) plane of the radical backbone. This is best illustrated in Figure 4 where we plot the two relevant parameters characterizing the two above-mentioned features for each level of theory. The dihedral angle $O_1-C_2-C_4-C_6$ determines the rotation angle of the almost planar $O_1-O_3-C_2-C_4$ constellation with respect to the planar conformation at 180° (see Figure 4). We observe an almost linear behavior between the nonplanarity of the radical backbone and the CO_2-rotation. This is a very striking result, which can be explained by considering the π-system of the CO_2 group. When the position of this group would not be influenced by attracting

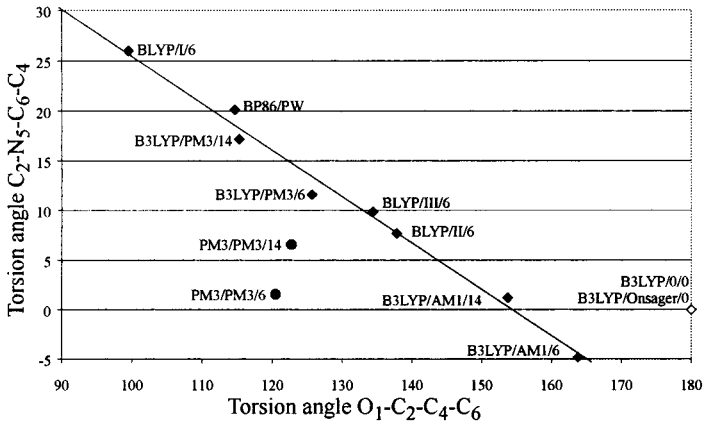

Figure 4. Relation between the torsion angle $O_1-C_2-C_4-C_6$ with respect to the $C_2-N_5-C_6-C_4$ angle in the various optimized geometries, obtained at different levels of theory: the ONIOM or ab initio optimized geometries (◆) and the purely semiempirical optimized geometries (●). In addition, the results of earlier theoretical calculations are indicated (◇).

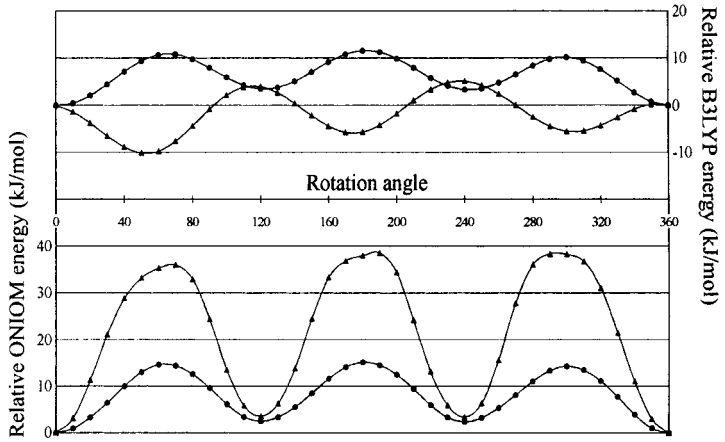

Figure 5. B3LYP/631G** energies versus ONIOM-extrapolated energies relative to the energy of the optimized B3LYP/PM3/14 geometry as a function of the rotation angle for both the methyl (●) and amino (▲) group (ONIOM-extrapolated energy = −324.877522 au; B3LYP/631G** energy = −323.034459 au).

hydrogen bonds, the associated π-cloud would be oriented parallel to the lone electron orbital (LEO) on carbon C_4. The LEO conjugates with the π-cloud of CO_2 and the radical carbon center is stabilized by the effect of resonance stabilization. However, when strong hydrogen bonds force the CO_2 group to shift out of the plane of the radical backbone, the π-cloud gets rotated relative to the direction of the LEO and is no longer parallel, resulting in a diminished conjugation. Since, in this case, sp^2 hybridization of the C_4 carbon does not cause an overall stabilization of the radical, the atom has some sp^3 character as well. Methods which substantially differ from this quasi-linear pattern (Figure 4) are systematically of lower level of theory. Both PM3/PM3/6−14 models describe the central molecule within the semiempirical approach of PM3, which is clearly insufficient.

Concluding, the deviation from planarity of the radical backbone is a direct consequence of the appearance of hydrogen bridges which induce a rotation of the CO_2 group, forcing the radical center to a nonplanar conformation. It should be stressed that the strong hydrogen bonds only take place between the oxygen atoms and the amino protons, which is clearly seen in the Figures 2 and 3. Methyl protons are not involved in any hydrogen bond and remain submitted to quasi-free rotations, in contrast to the amino protons whose internal rotations are completely hindered by the hydrogen bonds. The strength of the hydrogen bond is a determining factor to which extent the radical backbone deviates from planarity. The intermolecular hydrogen bridges coming into play are composed of oxygen and hydrogen atoms belonging to the central molecule and one of the neighbors. The levels of theory at which the central radical and the environment are described may differ. The PM3/PM3/6−14 and layered B3LYP/PM3/6−14 methods rely on the semiempirical PM3-method for the description of the relevant hydrogen bridges, while the layered B3LYP/AM1/6−14 models are based on the AM1 Hamiltonian.

The effect of the molecular environment on the optimized geometry is illustrated in Figure 5, where the relative B3LYP- and ONIOM-extrapolated energies are plotted as a function of the rotation angle of both the methyl and amino group. This plot was obtained by gradually rotating the methyl and amino group, starting from the B3LYP/PM3/14 optimized geometry, while keeping all other geometrical parameters fixed. Quite striking in this figure is the fact that the starting geometry at 0° (the B3LYP/PM3/14 optimized geometry) does not represent a minimum for the amino group rotation (marked ▲). On the other hand, the ONIOM-extrapolated energy of the starting geometry turns out to be a minimum, since in this case the molecular environment is included. The surrounding alanine molecules force the central radical to a conformation that does not correspond to an energetically most-favored structure in vacuo. A similar effect is not observed for the methyl group rotation, indicating that this internal motion is a quasi-free rotation in the crystal lattice.

TABLE 3: Summary of the Isotropic and Anisotropic Components of the Hyperfine Coupling Tensor[a]

	experimental				B3LYP/0/0				B3LYP/Onsager/0				PM3/PM3/14				PM3/PM3/6			
	A_{iso}	A_{xx}	A_{yy}	A_{zz}	A_{iso}	A_{xx}	A_{yy}	A_{zz}	A_{iso}	A_{xx}	A_{yy}	A_{zz}	A_{iso}	A_{xx}	A_{yy}	A_{zz}	A_{iso}	A_{xx}	A_{yy}	A_{zz}
O1													−2.6	−51.4	19.8	23.7	−0.4	−47.5	21.3	25.1
C2													−28.6	−34.5	−26.0	−25.2	−30.7	−36.4	−28.1	−27.5
O3													−0.7	−44.7	18.7	23.9	−2.6	−61.9	25.5	28.7
C4					94.0	16.5	17.6	247.9					82.0	12.0	13.8	220.1	71.5	3.7	5.1	205.7
N5	7.3	5.5	8.2	8.3	−8.0	−8.5	−7.8	−7.6					−3.7	−4.1	−3.8	−3.2	−6.5	−6.7	−6.6	−6.1
C6					−31.6	−34.0	−32.0	−29.7					−28.9	−30.9	−29.0	−26.8	−28.7	−30.4	−29.1	−26.6
H7	70.8	67.9	68.1	76.4	68.4	63.7	64.6	76.9	95.5	90.9	92.1	103.5	114.3	109.8	111.4	121.5	61.4	57.4	58.2	68.5
H8									2.2	−1.9	−1.7	10.2	11.6	7.7	8.1	19.1	6.5	2.6	3.5	13.5
H9									95.7	91.1	92.3	103.7	53.9	49.8	50.2	61.6	111.7	107.8	108.5	118.8
H10	86.3	79.4	83.6	95.8	80.3	74.8	75.5	90.6	86.0	81.2	81.5	95.3	86.8	81.6	82.0	96.7	76.2	70.9	71.5	86.3
H11	10.2	5.3	5.4	19.9	13.9	8.7	9.5	23.5	12.0	7.1	7.5	21.4	12.1	6.5	7.7	22.0	8.0	2.8	3.9	17.2
H12	30.2	24.1	25.5	40.9	29.9	24.0	24.6	41.2	30.0	24.4	25.1	40.6	23.8	18.4	19.2	33.7	32.6	27.9	28.1	41.9

	B3LYP/PM3/14				B3LYP/PM3/6				B3LYP/AM1/14				B3LYP/AM1/6				BLYP/I/6			
	A_{iso}	A_{xx}	A_{yy}	A_{zz}	A_{iso}	A_{xx}	A_{yy}	A_{zz}	A_{iso}	A_{xx}	A_{yy}	A_{zz}	A_{iso}	A_{xx}	A_{yy}	A_{zz}	A_{iso}	A_{xx}	A_{yy}	A_{zz}
O1	−0.9	−38.5	14.1	21.7	−0.7	−38.5	13.8	22.4	−2.1	30.6	10.1	14.1	−1.0	−30.1	11.3	15.8	1.0	−42.9	16.2	29.6
C2	−23.9	−31.4	−21.5	−18.8	28.4	−36.5	−25.2	−23.4	−32.8	−41.4	−29.4	−27.6	−33.1	−42.3	−29.7	−27.4	−21.0	−29.8	−17.5	−15.7
O3	−4.8	−54.3	18.6	21.4	−6.2	−68.3	23.1	26.5	−4.8	−53.3	17.0	21.9	−6.6	−64.7	19.7	25.3	−10.7	−116.7	39.6	45.1
C4	152.3	84.5	86.0	286.4	116.9	50.0	51.2	249.7	81.2	8.5	9.7	225.4	74.5	4.2	5.1	214.1	271.9	222.8	224.8	368.1
N5	7.7	6.9	7.5	8.7	2.7	2.1	2.5	3.5	−7.2	−7.6	−7.3	−6.6	−8.4	−8.7	−8.7	−7.9	15.5	14.5	15.1	16.9
C6	−21.7	−23.8	−22.4	−19.0	−25.4	−27.3	−25.7	−23.2	−28.6	−30.6	−28.4	−26.8	−25.2	−27.1	−25.3	−23.1	−7.0	−9.1	−8.3	−3.7
H7	100.2	96.2	98.0	106.4	90.4	86.4	88.0	96.8	95.9	91.4	92.6	103.6	77.2	72.8	73.8	85.1	58.8	55.8	57.4	63.1
H8	4.2	0.0	0.3	12.2	2.0	−1.9	−1.6	9.6	2.8	−1.2	−1.0	10.7	1.7	−2.3	−1.8	9.3	0.8	−2.6	−1.7	6.8
H9	54.5	50.2	50.3	63.1	69.0	64.8	65.1	77.0	81.7	77.3	78.3	89.3	95.7	91.6	92.7	102.7	23.8	19.9	20.3	31.0
H10	84.6	80.3	80.9	92.7	80.7	76.3	76.8	88.9	4.5	−0.9	−0.3	14.8	2.7	−2.5	−1.7	12.5	61.3	58.4	58.8	66.7
H11	5.2	−0.5	0.8	15.3	4.8	−0.5	0.6	14.3	65.9	61.4	61.6	74.7	65.7	61.1	61.3	74.8	−1.4	−6.0	−4.6	6.4
H12	17.6	11.8	12.9	28.2	22.3	16.9	17.8	32.3	72.3	67.0	67.7	82.2	69.8	65.1	65.6	78.9	10.4	6.1	7.0	18.2

	BLYP/II/6				BLYP/III/6				BP86/PW			
	A_{iso}	A_{xx}	A_{yy}	A_{zz}	A_{iso}	A_{xx}	A_{yy}	A_{zz}	A_{iso}	A_{xx}	A_{yy}	A_{zz}
O1	0.1	−43.5	15.2	28.6	−1.2	−39.8	13.9	22.2	−1.8	−47.2	16.7	25.0
C2	−35.1	−45.7	−30.8	−28.7	−31.2	−40.1	−27.7	−25.8	−23.8	−32.3	−21.4	−17.5
O3	−8.7	−90.5	30.4	33.9	−4.7	−63.4	23.1	26.4	−4.0	−50.7	17.8	20.9
C4	84.7	21.7	22.7	209.8	99.0	31.0	32.4	233.7	143.4	77.4	79.1	273.7
N5	−2.0	−2.4	−2.2	−1.5	−1.6	−2.2	−1.8	0.9	6.6	5.6	6.4	7.8
C6	−24.9	−26.6	−24.6	−23.4	−26.7	−28.7	−26.6	−24.9	−20.9	−22.7	−21.7	−18.3
H7	71.6	67.6	69.1	78.1	84.7	80.4	82.1	91.6	105.1	101.3	102.8	111.1
H8	1.6	−2.2	−1.1	8.0	1.4	−2.5	−1.9	8.5	9.6	5.7	6.0	17.1
H9	74.9	71.1	71.6	82.1	77.8	73.6	74.2	85.7	41.0	36.8	37.0	49.2
H10	74.3	70.1	70.5	82.4	85.1	80.6	81.0	93.7	95.2	90.9	91.7	103.2
H11	4.9	0.0	1.1	13.7	6.0	0.7	1.9	15.3	6.7	1.3	2.8	16.0
H12	26.4	21.9	22.3	35.0	30.0	25.0	25.5	39.3	17.0	11.4	12.6	27.0

[a]Values were measured in MHz, calculated at the B3LYP/6-311G** level for all atoms in the R2 radical, and optimized at different levels of theory. Experimental values were taken from ref 7.

3.2. EPR Parameters. For all optimized geometries, the EPR parameters of the central radical have been calculated at the B3LYP/6311G** level of theory. This means that for each optimized geometry of the central radical, we have recalculated the electronic wave functions at a high and uniform level in order to get EPR parameters constructed on the same basis. This allows us to attribute differences in the behavior of the EPR-parameters to geometrical features rather than to methodological grounds. The results are listed in Table 3. The partial sp^3 character of the radical center C_4 in most optimized geometries has a considerable effect on the EPR hyperfine coupling constants of the surrounding atoms. In Figure 6 the hfcc of nitrogen, calculated at the different levels of theory is plotted as a function of the improper torsion angle $C_2-N_5-C_6-C_4$, which stands for a measure of deviation from planarity of the radical backbone. The plot indicates that the N hfcc exhibits an almost linear dependence with the nonplanarity of the radical backbone: the more the radical backbone deviates from the planar conformation, the larger the N-hfcc prediction becomes. The experimental value of 7.3 MHz[7] is best reproduced by the B3LYP/PM3/14 and the periodic BP86/PW calculations. Only few calculations succeed in reproducing the N-hfcc in a satisfactory way. The two B3LYP/AM1 models even underestimate the experimental value by 14 to 15 MHz. The striking correlation between the hfcc of the nitrogen atom and the nonplanarity of the radical backbone is confirmed by additional calculations based on models whose ab initio prediction of the N-hfcc differs significantly from the experimental value but where we constraint the improper torsional angle $C_2-N_5-C_6-C_4$ to be 17.22°, as resulting from the B3LYP/PM3/14 optimized geometry. Applied to the BLYP/I/6 optimized geometry, we get a value for the N-hfcc (indicated by the asterisk * in Figure 6) close to the experimental estimate and obeying the linear correlation, as suggested.

As the methyl group acts as a quasi-free rotor even in a crystalline environment (we refer to the discussion on this item) only computed averages of the methyl proton couplings have sense. Their absolute differences between calculated and experimental isotropic coupling constants are displayed in Figure 7 for all optimized geometries. A striking feature is the excellent reproduction of these average hfcc's by the calculations in the absence of any neighbors. All cluster and periodic models

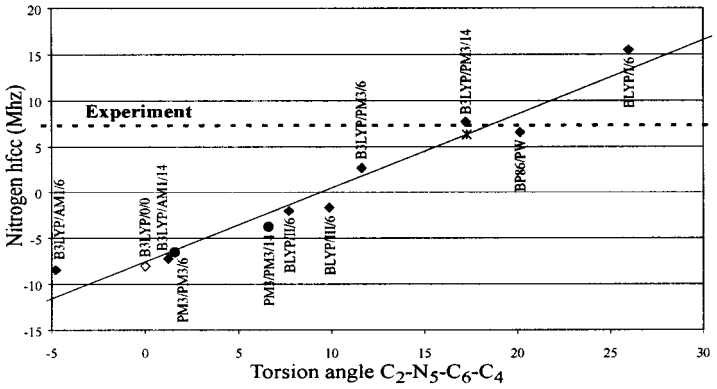

Figure 6. The nitrogen hyperfine coupling constant is plotted as a function of the torsion angle $C_2-N_5-C_6-C_4$ at different levels of theory. The dotted line represents the experimental value, while the asterisk (*) stands for the B3LYP/I/6 result with a constraint on the improper torsion angle $C_2-N_5-C_6-C_4$ (see text). The other symbols conform to the conventions in Figure 4.

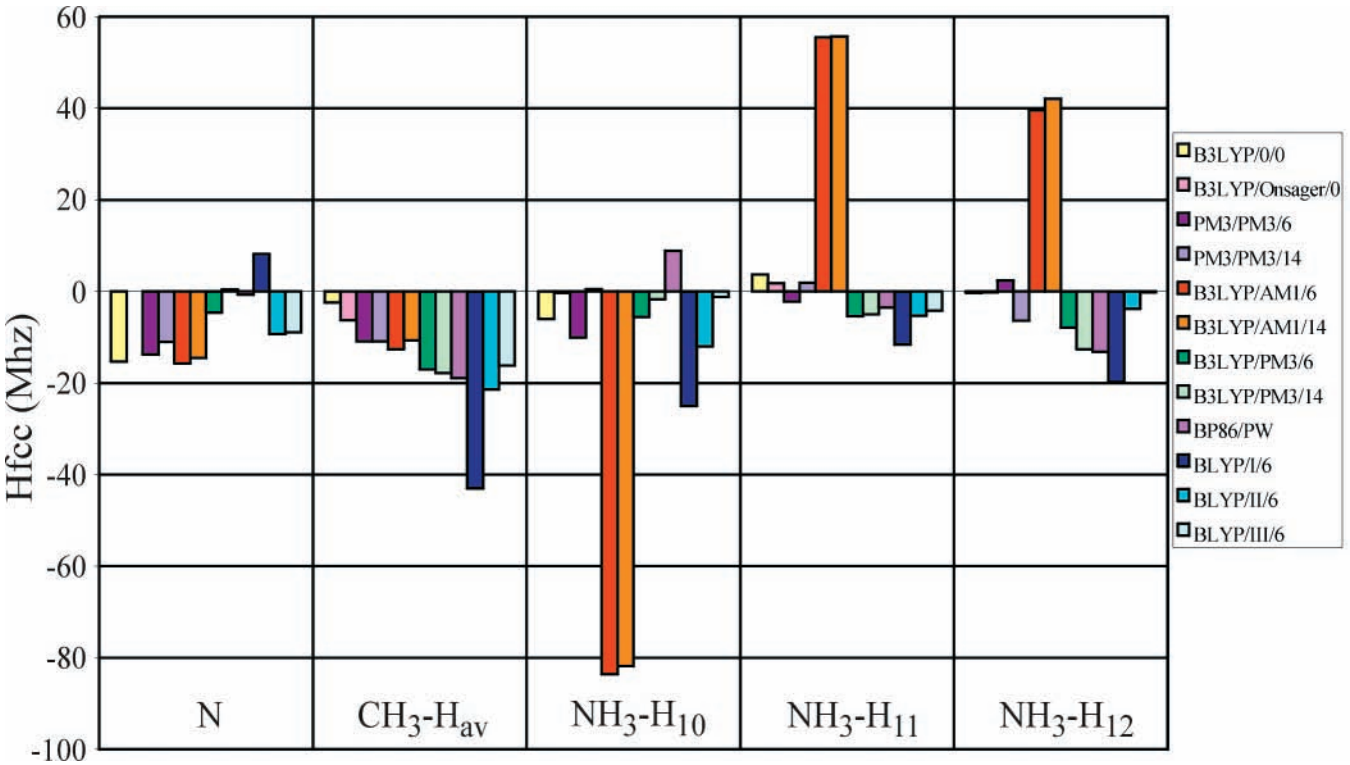

Figure 7. Overview of the different hyperfine coupling constants calculated at various levels of theory relative to the experimental values. Note that the B3LYP/Onsager/0 prediction for the N-hfcc has not been reported in ref 14 and accordingly not indicated.

predict values which are not of that level of agreement. This is an unlike feature, as this points toward the necessity of a planar-radical structure for getting satisfactory reproduction of the methyl proton hfcc's, and is apparently in contrast to preceding conclusions. This stimulated us to study into more detail the underlying reasons of this apparent contradiction. Therefore we performed some additional calculations in an attempt to search for the geometrical parameters with the greatest impact on the averaged value of the methyl hydrogen coupling constants. Starting from the B3LYP/PM3/14 optimized geometry, the planarity of the radical is gradually increased by reducing the improper torsional angle $C_2-N_5-C_6-C_4$ to zero, while keeping all other variables at their optimized values. In a subsequent step, the CO_2 group is rotated gradually toward a fully planar conformation of the radical backbone. During these geometry changes, the average methyl proton hfcc values are systematically calculated and reported in Figure 8. In the first part of the figure, the average hfcc is plotted versus the improper torsion angle $C_2-N_5-C_6-C_4$ reflecting the measure of nonplanarity of the radical backbone. This change in geometry already induces an increase of 10 MHz. In the second part of the figure, the isotropic hfcc is shown with respect to the $O_1-C_2-C_4-N_5$ torsional angle. This rotation of the CO_2 group toward planarity gives rise to an additional increase of 5 MHz. The remaining discrepancy between the experimental and the average methyl proton hfcc can probably be attributed to the other geometrical parameters that were not optimized. This calculation suggests that the experimental (rotationally averaged) value of the methyl proton hfcc originates from a planar radical structure, as suggested by both experimental and earlier theoretical studies.[12,14] We believe that this apparent contradiction with earlier conclusions is due to temperature effects on the geometry of the central radical. All our calculations have been performed without accounting for finite temperature effects, our optimized geometries represent structures of the radical at 0 K. The minimal energy conformation is in most cases a nonplanar

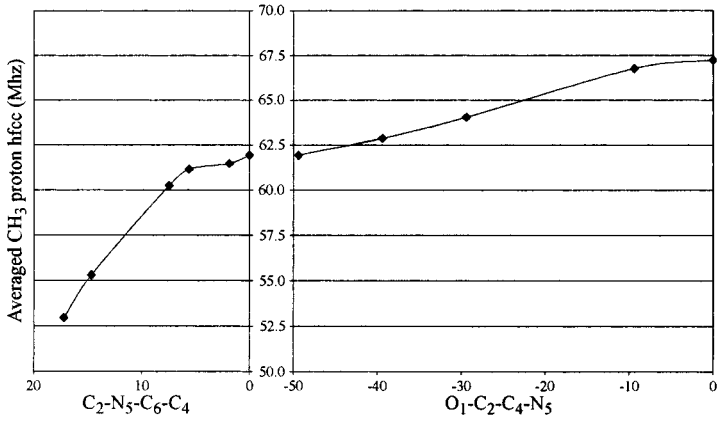

Figure 8. The averaged methyl proton hyperfine coupling constants as a function of the planarity of the radical backbone and rotation of the CO_2 group.

structure. Experimental hfcc values, on the other hand, are all recorded at room temperature and have been assigned to a planar radical structure. As a hypothesis it might therefore be put forward that at 0 K, the radical resides in a nonplanar conformation, in which the hydrogen bonds between the oxygens of the central CO_2 group and the hydrogens of the surrounding alanine molecules are minimal, resulting in a rotation of the CO_2 group and a nonplanarity of the radical backbone. By increasing the temperature, all vibrational modes are more excited due to thermal agitation. This will decrease the strength of the hydrogen bonds, and the average energy of the radical is high enough to move away from its ground-state structure at 0 K. Consequently, the CO_2 group can rotate toward a more planar structure of the radical backbone and the C_4 carbon center will also evolve to planarity. Further theoretical and experimental work is needed in order to sustain previous assumptions. In this context, molecular dynamics calculations at room temperature are in progress in order to determine the radical structure at more elevated temperatures.

The situation is different for the amino protons. Their isotropic hyperfine coupling constants are also displayed in Figure 7. The amino protons are involved in intermolecular hydrogen bridges. Each proton participates in one hydrogen bond with an oxygen atom from a neighboring alanine molecule. Due to steric hindrance caused by hydrogen atoms of the nearest molecular neighbors in the crystal lattice, the amino group cannot freely rotate, resulting in three, individual, hyperfine coupling tensors for the amino protons. Hydrogen bond distances fluctuate around 1.8 Å, except for the B3LYP/AM1/6−14 structures where they are overestimated (see discussion on this matter). The hydrogen bonds cause a rotation of the amino group about the C_4-N_5 axis. This torsional motion is described by the dihedral angle $H_{10}-N_5-C_4-C_2$. From Table 2, it follows that most levels of theory yield comparable values for this dihedral angle. Apart from the B3LYP/AM1/6−14 levels and the BLYP/I/6 level, the torsional angle always varies between 70° and 80°. In the case of BLYP/I/6 the small deviation can most likely be attributed to basis size effects. The B3LYP/AM1/6−14 values differ significantly, as could be expected from the overestimated hydrogen bond lengths. In earlier studies by Lahorte et al.[12] and Ban et al.,[14] a geometry was proposed in which one of the hydrogen atoms of the amino group lies in the plane of the fully planar radical backbone. To get good agreement with experimental results, the amino group had to be rotated about the C_4-N_5 axis. The final geometries proposed in ref 12 and ref 14 show a dihedral angle $H_{10}-N_5-C_4-C_2$ of approximately 80°, which is in close agreement with our ab initio results. Apparently, by accounting for the molecular environment of the central radical this "manual" adjustment of the amino group rotation is no longer necessary.

The overview of the different results and discrepancies with experiment in Figure 7 learns that most of the cluster and the periodic calculations succeed in a very satisfactory reproduction of the amino-proton hfcc's. Two calculations emerge from the general pattern: those corresponding to the B3LYP/AM1/6−14 methods. Their optimized geometries are very unrealistic, as already mentioned, and they obviously result into large discrepancies as noticed in the coupling constants of the three amino protons. The PM3/PM3/14, B3LYP/PM3/6−14, and BP86/PW geometries produce a comparable absolute error over all amino proton hfcc's (15 to 25 MHz in total). The calculated amino proton hfcc's for the PM3/PM3/6 geometry are in somewhat better agreement with experiment, although the error is still quite large for proton H_{12}. Figure 7 also shows that the size of the basis set has a substantial impact on the accuracy of the results. Among the three B3LYP/I−III/6 geometries, the best agreement with experiment is reached by the model corresponding to the most extended basis set. This is probably due to a more reliable reproduction of the hydrogen bridges.

We are not going into detail on the anisotropic couplings, since they generally behave as the isotropic contributions. For completeness, they are also shown in Table 3.

4. Conclusions

The geometries and hyperfine coupling constants of the R2 radical of L-α-alanine have been computed using primarily density functional theory in both cluster and periodic models. The calculated results have been compared with the experimental values obtained from X-irradiated crystals of L-α-alanine at 295 K. A detailed investigation has been conducted on the optimized geometries in a variety of models using different levels of theory and their impact on the various hyperfine coupling constants. This work can be regarded as an extension of previously done work,[12,14] where the lack of environmental effects was commonly accepted as inadequate for an accurate description and reproduction of quantities that are strongly geometry-dependent. The most dramatic change in the geometry due to the crystal environment on the alanine radical in its zwitterionic form is the deviation of the radical backbone from its planar skeleton. This deviation of planarity is a prerequisite for the satisfactory reproduction of the isotropic hyperfine coupling constants of the nitrogen atom and the amino protons. On the other hand the nonplanarity hinders the reproduction of the experimental-

averaged methyl proton hfcc's. We attribute this discrepancy to temperature effects, since the static calculations correspond to a situation at zero temperature, while the experimental measurement took place at room temperature. Thermal agitation probably weakens the strength of the intermolecular hydrogen bridges, breaking down the forces keeping the central radical R2 in the nonplanar conformation. This picture would suggest a tendency to a more planar structure as the average conformation, giving a probable interpretation of the relatively good results obtained from the B3LYP/0/0 and B3LYP/Onsager/0 calculations on isolated molecules. We stress the overall success of the periodic calculations. They have posed considerably less convergence problems than most of the cluster calculations. The optimized geometries resemble those of the most advanced cluster results and the overall agreement with the experimental hfcc's should be emphasized and is best illustrated in Figure 7.

Methodologically, this study shows that accounting for the molecular environment is of crucial importance for the accurate modeling of the radical geometry and the reproduction and prediction of EPR hyperfine coupling constants of organic alanine radicals. Density-functional theory provided a powerful computational tool in this respect. It might be expected that the approach adopted in this work is suitable for the study of other organic radicals in the crystal phase.

Acknowledgment. This work is supported by the Fund for Scientific Research−Flanders (FWO) and the Research Board of Ghent University.

References and Notes

(1) McLaughlin, W. L.; Taylor, D. M. *Appl. Radiat. Isotopes* **1996**, *47*, 1.

(2) Muto, H.; Iwasaki, M. *J. Chem. Phys.* **1973**, *59*, 4821. Kuroda, S.; Miyagawa, I. *J. Chem. Phys.* **1982**, *76*, 3933. Itoh, K.; Miyagawa, I. *J. Mol. Struct.* **1988**, *190*, 85. Vanhaelewyn, G. C. A. M.; Mondelaers, W. K. P. G.; Callens, F. J. *Radiat. Res.* **1999**, *151*, 590. Vanhaelewyn, G. C. A. M.; Amira, S. A.; Mondelaers, W. K. P. G.; Callens, F. J. *Spectrochim. Acta A* **2000**, *56*, 387.

(3) Simmons, J. A. *J. Chem. Phys.* **1962**, *36*, 469. Arber, J. M.; Sharpe, P. H. G.; Joly, H. A.; Morton, J. R.; Preston, K. F. *Appl. Radiat. Isotop.* **1991**, *42*, 665. Ciesielski, B.; Wielopolski, L. *Radiat. Res.* **1994**, *140*, 105.

(4) van Roggen, A.; van Roggen, L.; Gordy, W. *Bull. Am. Phys. Soc.* **1956**, *1*, 266.

(5) Miyagawa, I.; Gordy, W. *J. Chem. Phys.* **1960**, *32*, 255.

(6) Miyagawa, I.; Itoh, K. *J. Chem. Phys.* **1962**, *36*, 2157. Matsuki, K.; Miyagawa, I. *J. Chem. Phys.* **1982**, *76*, 3945.

(7) Sagstuen, E.; Hole, E. O.; Haugedal, S. R.; Nelson, W. H. *J. Phys. Chem. A* **1997**, *101*, 9763.

(8) Tortonda, F. R.; Pascual-Ahuir, J. L.; Silla, E.; Tuñon, I. *Chem. Phys. Lett.* **1996**, *260*, 21. Tarakeshwar, P.; Manogaran, S. *J. Mol. Struct. (THEOCHEM)* **1997**, *417*, 255. Rega, N.; Cossi, M.; Barone, V. *J. Am. Chem. Soc.* **1998**, *120*, 5723. Tortonda, F. R.; Pascual-Ahuir, J.; Silla, E.; Tuñon, I.; Ramirez, F. J. *J. Chem. Phys.* **1998**, *109*, 592. Sambrano, J. R.; de Sousa, A. R.; Queralt, J. J.; Andres, J.; Longo, E. *Chem. Phys. Lett.* **1998**, *294*, 1. Chakraborty, D.; Manogaran, S. *Chem. Phys. Lett.* **1998**, *294*, 56.

(9) Ding, Y.; Krogh-Jespersen, K. *Chem. Phys. Lett.* **1992**, *199*, 261.

(10) Barone, V.; Adamo, C.; Grand, A.; Subra, R. *Chem. Phys. Lett.* **1995**, *242*, 351.

(11) Wetmore, S. D.; Boyd, R. J.; Eriksson, L. A. *J. Phys. Chem. B* **1998**, *102*, 7674. Lahorte, P.; De Proft, F.; Callens, F.; Geerlings, P.; Mondelaers, W. *J. Phys. Chem. A* **1999**, *103*, 11130.

(12) Lahorte, P.; De Proft, F.; Vanhaelewyn, G.; Masschaele, B.; Cauwels, P.; Callens, F.; Geerlings, P.; Mondelaers, W. *J. Phys. Chem. A* **1999**, *103*, 6650.

(13) Lehmann, M. S.; Koetzle, T. F.; Hamilton, W. C. *J. Am. Chem. Soc.* **1972**, *94*, 2657.

(14) Ban, F.; Wetmore, S. D.; Boyd, R. J. *J. Phys. Chem. A* **1999**, *103*, 4303.

(15) Onsager, L. *J. Am. Chem. Soc.* **1936**, *58*, 1486. Wong, M. W.; Frisch, M. J.; Wiberg, K. B. *J. Am. Chem. Soc.* **1991**, *113*, 4776. Wong, M. W.; Wiberg, K. B.; Frisch, M. J. *J. Chem. Phys.* **1991**, *95*, 8991. Wong, M. W.; Wiberg, K. B.; Frisch, M. J. *J. Am. Chem. Soc.* **1992**, *114*, 523. Wong, M. W.; Wiberg, K. B.; Frisch, M. J. *J. Am. Chem. Soc.* **1992**, *114*, 1645.

(16) Saebo, S.; Klewe, B.; Samdal, S. *Chem. Phys. Lett.* **1983**, *97*, 499.

(17) Almlöf, J.; Kvick, A.; Thomas, J. O. *J. Chem. Phys.* **1973**, *59*, 3901. Bridet, J.; Fliszár, S.; Odiot, S.; Pick, R. *Int. J. Quantum Chem.* **1983**, *24*, 687. Mombourquette, M. J.; Weil, J. A.; Mezey, P. G. *Can. J. Chem.* **1984**, *62*, 21. Ángyán, J. G.; Silvi, B. *J. Chem. Phys.* **1987**, *86*, 6957. Helgaker, T. U.; Klewe, B. *Acta Chem. Scand. A* **1988**, *42*, 269. Popelier, P.; Lenstra, A. T. H., Van Alsenoy, C.; Geise, H. J. *Acta Chem. Scand. A* **1988**, *42*, 539. Popelier, P.; Lenstra, A. T. H.; Van Alsenoy, C.; Geise, H. J. *J. Am. Chem. Soc.* **1989**, *111*, 5658. Popelier, P.; Lenstra, A. T. H., Van Alsenoy, C.; Geise, H. J. *Struct. Chem.* **1991**, *2*, 3.

(18) Fülscher, M. P.; Mehler, E. L. *J. Comput. Chem.* **1991**, *12*, 811. Liao, M.; Zhang, Q. *J. Solid State Chem.* **1999**, *146*, 239.

(19) Car, R.; Parrinello, M. *Phys. Rev. Lett.* **1985**, *55*, 2471.

(20) For an example of a reference work, see: Levine, I. N. *Quantum Chemistry;* Prentice Hall: New Jersey, 1991, Chapter 16.

(21) Stewart, J. J. P. *J. Comput. Chem.* **1989**, *10*, 209. Stewart, J. J. P. *J. Comput. Chem.* **1989**, *10*, 221.

(22) Frisch, M. J.; Trucks, G. W.; Schlegel, H. B.; Scuseria, G. E.; Robb, M. A.; Cheeseman, J. R.; Zakrzewski, V. G.; Montgomery, J. A., Jr.; Stratmann, R. E.; Burant, J. C.; Dapprich, S.; Millam, J. M.; Daniels, A. D.; Kudin, K. N.; Strain, M. C.; Farkas, O.; Tomasi, J.; Barone, V.; Cossi, M.; Cammi, R.; Mennucci, B.; Pomelli, C.; Adamo, C.; Clifford, S.; Ochterski, J.; Petersson, G. A.; Ayala, P. Y.; Cui, Q.; Morokuma, K.; Malick, D. K.; Rabuck, A. D.; Raghavachari, K.; Foresman, J. B.; Cioslowski, J.; Ortiz, J. V.; Stefanov, B. B.; Liu, G.; Liashenko, A.; Piskorz, P.; Komaromi, I.; Gomperts, R.; Martin, R. L.; Fox, D. J.; Keith, T.; Al-Laham, M. A.; Peng, C. Y.; Nanayakkara, A.; Gonzalez, C.; Challacombe, M.; Gill, P. M. W.; Johnson, B. G.; Chen, W.; Wong, M. W.; Andres, J. L.; Head-Gordon, M.; Replogle, E. S.; Pople, J. A. *Gaussian 98*, revision A.7; Gaussian, Inc.: Pittsburgh, PA, 1998.

(23) Maseras, F.; Morokuma, K. *J. Comput. Chem.* **1995**, *16*, 1170. Svensson, M.; Humbel, S.; Froese, R. D. J.; Matsubara, T.; Sieber, S.; Morokuma, K. *J. Phys. Chem.* **1996**, *100*, 19357. Humbel, S.; Sieber, S.; Morokuma, K. *J. Chem. Phys.* **1996**, *105*, 1959. Matsubara, T.; Sieber, S.; Morokuma, K. *Int. J. Quantum Chem.* **1996**, *60*, 1101. Dapprich, S.; Komaromi, I.; Byun, K. S.; Morokuma, K.; Frisch, M. J. *J. Mol. Struct. (THEOCHEM)* **1999**, *462*, 1.

(24) For an example of a reference work, see: Parr, R. G.; Yang, W. *Density-Functional Theory of Atoms and Molecules;* Oxford University Press: New York, 1989.

(25) Becke, A. D. *J. Chem. Phys.* **1996**, *104*, 1040.

(26) Wong, M. W.; Radom, L. *J. Phys. Chem. A* **1998**, *102*, 2237. Parker, C. L.; Cooksy, A. L. *J. Phys. Chem. A* **1998**, *102*, 6186. Smith, D. M.; Nicolaides, A.; Golding, B. T.; Radom, L. *J. Am. Chem. Soc.* **1998**, *120*, 10223. Lynch, B. J.; Fast, P. L.; Harris, M.; Truhlar, D. G. *J. Phys. Chem. A* **2000**, *104*, 4811. Van Speybroeck, V.; Van Neck, D.; Waroquier, M.; Wauters, S.; Saeys, M.; Marin, G. B. *J. Phys. Chem. A* **2000**, *104*, 10939.

(27) Hariharan, P. C.; Pople, J. A. *Theor. Chim. Acta* **1973**, *28*, 213. Francl, M. M.; Pietro, W. J.; Hehre, W. J.; Binkley, J. S.; Gordon, M. S.; DeFrees, D. J.; Pople, J. A. *J. Chem. Phys.* **1982**, *77*, 3654.

(28) Dewar, M. J. S.; Thiel, W. *J. Am. Chem. Soc.* **1977**, *99*, 4899. Dewar, M. J. S.; Thiel, W. *J. Am. Chem. Soc.* **1977**, *99*, 4907. Dewar, M. J. S.; McKee, M. L.; Rzepa, H. S. *J. Am. Chem. Soc.* **1978**, *100*, 3607. Davis, L. P.; Guidry, R. M.; Williams, J. R.; Dewar, M. J. S.; Rzepq, H. S. *J. Comput. Chem.* **1981**, *2*, 433. Dewar, M. J. S.; Zoebisch, E. G.; Healy, E. F. *J. Am. Chem. Soc.* **1985**, *107*, 3902. Dewar, M. J. S.; Reynolds, C. H. *J. Comput. Chem.* **1986**, *2*, 140.

(29) ADF 1999 Baerends, E. J.; Ellis, D. E.; Ros, P. *Chem. Phys.* **1973**, *2*, 41. Versluis, L.; Ziegler, T. *J. Chem. Phys.* **1988**, *88*, 322. te Velde, G.; Baerends, E. J. *J. Comput. Phys.* **1992**, *99*, 84. Guerra, F. C.; Snijders, J. G.; te Velde, G.; Baerends, E. J. *Theor. Chem. Acc.* **1998**, *99*, 391.

(30) Becke, A. D. *Phys. Rev. A* **1988**, *38*, 3098.

(31) Lee, C. T.; Yang, W. T.; Parr, R. G. *Phys. Rev. B* **1988**, *37*, 785. Miehlich, B.; Savin, A.; Stoll, H.; Preuss, H. *Chem. Phys. Lett.* **1989**, *157*, 200.

(32) See for example: Elsässer, C.; Fähnle, M.; Chan, C. T.; Ho, K. M. *Phys. Rev. B* **1994**, *49*, 13975. Warren, R. W.; Dunlap, B. I. *Chem. Phys. Lett.* **1996**, *262*, 384.

(33) The CP code employed in this work is under development by Dr. Franco Buda at the Free University of Amsterdam, The Netherlands.

(34) Car, P.; Parrinello, M. *Phys. Rev. Lett.* **1985**, *55*, 2471.

(35) Stich, I.; Car, R.; Parrinello, M.; Baroni, S. *Phys. Rev. B* **1989**, *39*, 4997.

(36) Ryckaert, J. P.; Ciccotti, G.; Berendsen, H. J. C. *J. Comput. Phys.* **1997**, *23*, 327.

(37) For reviews see: Gombas, P. *Die Statistischen Theorie des Atomes und Ihre Anwendungen;* Wien: Springer-Verlag: 1949. March, N. H. *Adv. Phys.* **1957**, *6*, 1. March, N. H. *Self-Consistent Fields in Atoms;* Oxford: Pergamon: 1975. Lieb, E. H. *Rev. Mod. Phys.* **1981**, *53*, 603.

(38) Perdew, J. P.; Zunger, A. *Phys. Rev. B* **1981**, *23*, 5048.
(39) Perdew, J. P. *Phys. Rev. B* **1986**, *33*, 8822.
(40) Becke, A. D. *J. Chem. Phys.* **1992**, *96*, 2155.
(41) Vanderbilt, D. *Phys. Rev. B* **1990**, *41*, 7892.
(42) Meier, R. J.; van Doremaele, G. H. J.; Iarlori, S.; Buda, F. *J. Am. Chem. Soc.* **1994**, *116*, 7274. Tarazona, A.; Koglin, E.; Buda, F.; Coussens, B. B.; Renkema, J.; van Heel, S.; Meier, R. J. *J. Phys. Chem. B* **1997**, *101*, 4370.
(43) Barone, V.; Adamo, C.; Grand, A.; Jolibois, F.; Brunel, Y.; Subra, R. *J. Am. Chem. Soc.* **1995**, *117*, 12618. Barone, V. *Theor. Chim. Acta* **1995**, *91*, 113. Barone, V. *Chem. Phys. Lett.* **1996**, *262*, 201. Wetmore, S. D.; Boyd, R. J.; Eriksson, L. A. *J. Phys. Chem. B* **1998**, *102*, 5369. Wetmore, S. D.; Himo, F.; Boyd, R. J.; Eriksson, L. A. *J. Phys. Chem. B* **1998**, *102*, 7484. Wetmore, S. D.; Boyd, R. J.; Eriksson, L. A. *J. Phys. Chem. B* **1998**, *102*, 9332. Wetmore, S. D.; Boyd, R. J.; Eriksson, L. A. *J. Phys. Chem. B* **1998**, *102*, 10602.
(44) Krishnan, R.; Binkley, J. S.; Seeger, R.; Pople, J. A. *J. Chem. Phys.* **1980**, *72*, 650.
(45) Batra, R.; Giese, B.; Spichty, M.; Gescheidt, G.; Houk, K. N. *J. Phys. Chem.* **1996**, *100*, 18371.